Journal of Marine Science and Technology

Volume 23 | Issue 2 Article 2

NUMERICAL SIMULATION OF WATER ENTRY OF WEDGES BASED ON THE CIP METHOD

Zhao-Yu Wei
School of Naval Architecture and Ocean Engineering, Jiangsu University of Science and Technology, Zhenjiang, Jiangsu, P. R. China. School of Marine Engineering, Northwestern Polytechnical University, Xi'an, Shaanxi, P. R. China., weimuru@163.com

He-ye Xiao
No. 203 research institute of china ordnance industries, xi'an, P. R. China.

Zhi-dong Wang
School of Naval Architecture and Ocean Engineering, Jiangsu University of Science and Technology, Zhenjiang, Jiangsu, P. R. China.

Xiu-Hua Shi
School of Marine Engineering, Northwestern Polytechnical University, Xi'an, Shaanxi, P. R. China.

NUMERICAL SIMULATION OF WATER ENTRY OF WEDGES BASED ON THE CIP METHOD

Acknowledgements

The authors would like to thank the support of the Project Funded by the Priority Academic Program Development of Jiangsu Higher Education Institutions (PAPD).

Journal of Marine Science and Technology, Vol. 23, No. 2, pp. 142-150 (2015)
DOI: 10.6119/JMST-014-0206-2

NUMERICAL SIMULATION OF WATER ENTRY OF WEDGES BASED ON THE CIP METHOD

Zhao-Yu Wei[1, 3], He-ye Xiao[2], Zhi-dong Wang[1], and Xiu-Hua Shi[3]

Key words: water entry impact, wedge, constrained interpolation profile, THINC scheme.

ABSTRACT

The hydrodynamic problems for water entry of wedges are studied by a constrained interpolation profile (CIP) based on Cartesian grid method. The CIP scheme was applied to the Cartesian grid based on flow solver, which was first described. The tangent of hyperbola for interface capturing (THINC) scheme was applied to capture the free surface. The CIP method was extended to capture the dynamics in the water entry approach. The simulations were performed in three aspects. First, pressure distributions for the wedges entering into water with constant speed were predicted, and the results were compared with the similarity solutions by the boundary element method (BEM). Then simulations were conducted for the free-falling wedges entering into water with one degree of freedom. The results were compared with the published experimental data. Finally, the impact of a wedge on the water surface in a free fall motion with an initial heel angle was studied. The motion of the wedge was subjected to three degrees of freedom, and the results were also compared with those of experiments.

I. INTRODUCTION

Water entry impact problem has wide applications in ocean engineering. More than eighty years ago, Von Karman (1929) provided the first approximate solution for the load prediction as the V-shaped body impacts the water surface, thus initiated the field of fluid-structure impact. His work was further developed by Wagner (1932), who accounted the local up rise of water. Later, Dobrovolskaya (1969) obtained the first complete solution for a two-dimensional wedge entering into the water at constant velocity. His work was based on the velocity potential theory, where the gravity of fluid flow was ignored. Since there was no length scale, the fluid was self-similar. Zhao and Faltinsen (1993) reconsidered the problem and solved it using a boundary element method in the time domain. The thin jetting was cut to avoid numerical errors. Kihara (2004) also studied the water entry problem of wedges at constant speed. In his work, the boundary element method (BEM) and a mixed Euler and Lagrangian method (MEL) were employed, introducing an analytical description of the jetting flow. Other works on water entry problems of wedges include those by Semenov and Iafrati (2006) and Xu et al. (2008). For the free surface water entry, an important work was one by Wu et al. (2004). By using BEM with Taylor expansion for the jet, Wu et al. obtained the time marching solution for the water entry of a wedge in free fall motion. The solution was further expanded to three degrees of freedom by Xu et al. (2010).

Besides these potential-flow based methods, the recently developed computational fluid dynamics (CFD) methods have made it possible to solve the water entry problems and also treat highly distorted or breaking free surface breaking by solving the governing equations. Oger et al. (2006) solved the water entry of wedges using smoothed particles hydrodynamics (SPH) method. Other examples include the use of volume of fluid (VOF) for water entry problems by Kleefsman et al. (2005), and the level set as described by Yang and Stern (2009). In addition, the constrained interpolation profile (CIP) method was also applied to investigate the water entry problem. Zhu et al. (2007) applied the CIP method to study the water entry and exit of a two-dimensional horizontal circular cylinder. Yang and Qiu (2012) also used the same method to solve the water impact of two- and three-dimensional bodies.

In this work, the constrained interpolation profile (CIP) based Cartesian grid method is presented and applied to the water impact problems of wedges. The Cartesian grid method used for the numerical solution does not depend on the locations of the body boundary and the free surface, which makes the computation of strongly nonlinear problems with complicated free-surface deformation more efficient and convenient. In Sect. 2 we first give a brief description of the CIP-based flow solver. The THINC scheme (tangent of hyperbola for

Paper submitted 09/26/12; revised 01/07/14; accepted 02/06/14. Author for correspondence: Zhao-Yu Wei (e-mail: weimuru@163.com).
[1] *School of Naval Architecture and Ocean Engineering, Jiangsu University of Science and Technology, Zhenjiang, Jiangsu, P. R. China.*
[2] *No. 203 research institute of china ordnance industries, xi'an, P. R. China.*
[3] *School of Marine Engineering, Northwestern Polytechnical University, Xi'an, Shaanxi, P. R. China.*

interface capturing) for the interface capturing is also introduced and explained. To validate the CIP method and the THINC scheme for free surface capturing, the water entry of two-dimensional wedges were investigated. In Sect. 3.1, the water entry of wedges with constant speed is numerically simulated and compared with the similarity solution by the BEM. Then in Sect. 3.2 we present the numerical results of symmetry wedges entering water in free fall motion and the results are compared with that from experiments. In Sect. 3.3, the water impact of a wedge in free fall motion with an initial heel angle is studied and the results are also compared with experimental data.

II. NUMERICAL METHODS

1. Governing Equations

Assuming that there is no temperature variation in the problem, the flow is considered as unsteady, viscous and incompressible. The governing equations can therefore be written as

$$\frac{\partial u_i}{\partial x_i} = 0 \tag{1}$$

and

$$\frac{\partial u_i}{\partial t} + u_j \frac{\partial u_i}{\partial x_j} = -\frac{1}{\rho}\frac{\partial p}{\partial x_i} + \frac{1}{\rho}\frac{\partial}{\partial x_j}(2\mu S_{ij}) + f_i \,, \tag{2}$$

where $S_{ij} = (\partial u_i / \partial x_j + \partial u_j / \partial x_i)/2$, f_i stands for the gravity. Eq. (2) was solved by a fractional step method, in which the equation was divided into three calculation steps: one advection step and two non-advection steps (Hu and Kashiwagi, 2004). The CIP scheme was applied to calculate the advection step while the two non-advection parts were calculated by the Euler explicit scheme and the implicit scheme integration, respectively. The Poisson equation was used to obtain the pressure distribution, which was treated in a non-advection calculation step and can be written as

$$\frac{\partial}{\partial x_i}\left(\frac{1}{\rho}\frac{\partial p^{n+1}}{\partial x_i}\right) = \frac{1}{\Delta t}\frac{\partial u_i^{**}}{\partial x_i} \,, \tag{3}$$

here the superscript "n+1" stands for the quantities of the next time step, and "**" denotes interim values obtained from the first non-advection phase. After Eq. (3) was numerically solved, we were able to obtain the pressure distribution over the whole computation domain, where Eq. (3) was assumed valid. More details about the calculation of the Poisson equation and fractional step treatment used in the flow solver can be found in a previous study by Hu and Kashiwagi (2004).

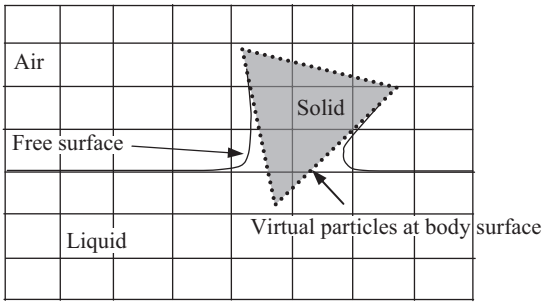

Fig. 1. Concept for the Cartesian grid approach during water entry of wedges.

2. The Inner Interface Treatment Method

The free surface and wedge boundary in the present numerical method were treated as immersed interfaces, as shown in Fig. 1. A density function ϕ_m was defined to recognize the different phases, in which m = 1, 2, 3 denote the liquid, gas and solid phases, respectively. Each computational cell satisfies the density function $\Sigma\phi_m$ =1.0.

The interfaces in the multiphase problem need to be determined in the computation, which can be performed by solving the following equation for the density function

$$\frac{\partial \phi_m}{\partial t} + u_i \frac{\partial \phi_m}{\partial x_i} = 0 \,. \tag{4}$$

Only two density functions need to be solved, e.g., ϕ_1 for the liquid and ϕ_3 for the solid; and the third can be obtained by

$$\phi_2 = 1 - \phi_1 - \phi_3 \,. \tag{5}$$

As all of the density functions are determined, any physical property λ, such as density and viscosity, can be obtained for each computation cell as

$$\lambda = \sum_{m=1}^{3} \phi_m \lambda_m \,. \tag{6}$$

In order to maintain numerical stability, the density and viscosity of the solid wedge are set to be the same as that of the liquid. Two kinds of interface should be considered; gas-liquid interface (free surface) and solid-fluid interface (wedge boundary). The THINC (tangent of hyperbola for interface capturing) scheme is applied to capture the free surface while the virtual particle method was applied to track the wedge surface (Hu and Kashiwagi, 2009). The THINC scheme has the features needed for our computations: mass conservation and effectivity in eliminating numerical diffusion and oscillation (Hu and Kashiwagi, 2009; Xiao et al., 2005, Zhao and Hu, 2012).

Eq. (4) can be integrated by an upwind scheme, such as the CIP scheme (Hu and Kashiwagi, 2004). The interface is then

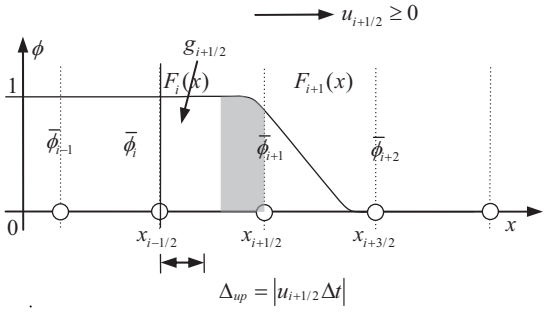

Fig. 2. Concept of THINC scheme.

determined by the iso-surface of ϕ = 0.5. Similar to CIP scheme, the profile of ϕ inside a computation cell is approximated by an interpolation function and the time integration of ϕ is performed by a semi-Lagrangian scheme. Instead of using a polynomial function as adopted by the CIP scheme, the THINC scheme uses a hyperbolic tangent function to approximate the profile (Xiao et al., 2005).

To explain the THINC scheme, a one-dimensional case is considered. The multi-dimensional calculation can be done using a directional splitting technique (Godunov, 1959). The advection equation on $\phi(x, t)$ for THINC scheme is written in a conservation form as

$$\frac{\partial \phi}{\partial t} + \frac{\partial (u\phi)}{\partial x} = 0 . \tag{7}$$

Integrating Eq. (7) over $[t, t + \Delta t]$ and $[x_{i-1/2}, x_{i+1/2}]$ gives

$$\bar{\phi}_i^{n+1} = \bar{\phi}_i^n + \left(g_{i-1/2} - g_{i+1/2}\right)/\Delta x_i , \tag{8}$$

where $\bar{\phi}_i = (1/\Delta x)\int_{x_{i-1/2}}^{x_{i+1/2}} \phi(x,t)dx$ is the cell averaged density function, $g_{i\pm1/2} = \int_t^{t+\Delta t} (u\phi)_{i\pm1/2}\, dt$ is the flux at the cell boundary. The flux is computed by a semi-Lagrangian scheme as shown in Fig. 2. The shaded area denotes the flux at $x = x_{i+1/2}$ for the case of $u_{i+1/2} > 0$.

Since the variation of $\phi\,(0 \leq \phi \leq 1)$ across the free surface is step-like, we can approximate the profile inside the computational cell $[x_{i-1/2}, x_{i+1/2}]$ by a piecewise modified hyperbolic tangent function as

$$F_i(x) = \alpha\left\{1 + \gamma \tanh[\beta((x - x_{i-1/2})/\Delta x_i - \delta)]\right\}/2 , \tag{9}$$

where $\Delta x_i = x_{i+1/2} - x_{i-1/2}$, and α, β, γ, δ are the parameters to be specified. Parameter β controls the steepness of the profile, and a value of β = 3.5 was used in the present computations. Parameter δ represents the middle point of the hyperbolic tangent function and was determined by the following relation

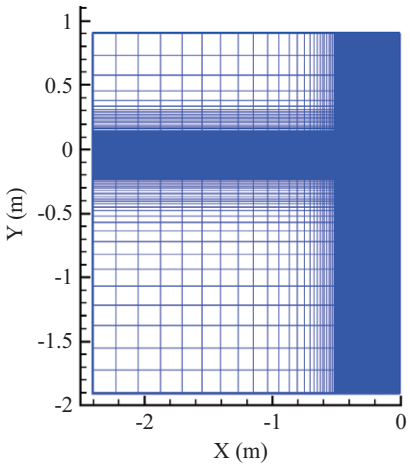

Fig. 3. The configuration for the grid cells.

$$\frac{1}{\Delta x_i}\int_{x_{i-1/2}}^{x_{i+1/2}} F_i(x)dx = \bar{\phi}_i^n . \tag{10}$$

After $F_i(x)$ was determined from Eq. (9), the flux across the cell boundaries was then calculated and the cell integrated value at a new time step $\bar{\phi}_i^{n+1}$ was computed. As this cell-integrated value was used to determine the free surface, the mass conservation of liquid is automatically satisfied.

III. NUMERICAL RESULTS AND DISCUSSIONS

Convergence study was first undertaken. The schematic illustration of the basic grid configuration for all the computations performed in this study is shown in Fig. 3. The grid spacing was varied, with the minimum but equally spaced cells at the region near the free surface in the y-direction and around the wedge in the x-direction. The cell size increased gradually away from the impact region and the free surface to reduce the CPU requirement and memory. The minimum grid spacing was 0.002 m, which was found to give indistinguishable results. Care was provided to ensure that there were at least five virtual particles within each grid cell. As a result, the size of the largest cell furthest away from the wedge was about 0.2 m. In the present model, calculations started for the wedges with a very small distance above the quiescent water surface. The wedge fell freely in at first, before it impacted the free surface of water.

1. Test Cases of Water Impact for Symmetric Wedges with Constant Speed

To validate the CIP method, we first applied it to the cases of symmetric wedges impacting the free surface with constant velocity. The results of our simulation were compared with the similarity solutions of BEM by Wu et al. (2004). The wedges used in the CIP method had the same side length of 0.305 m. Four deadrise angles were considered, corresponding

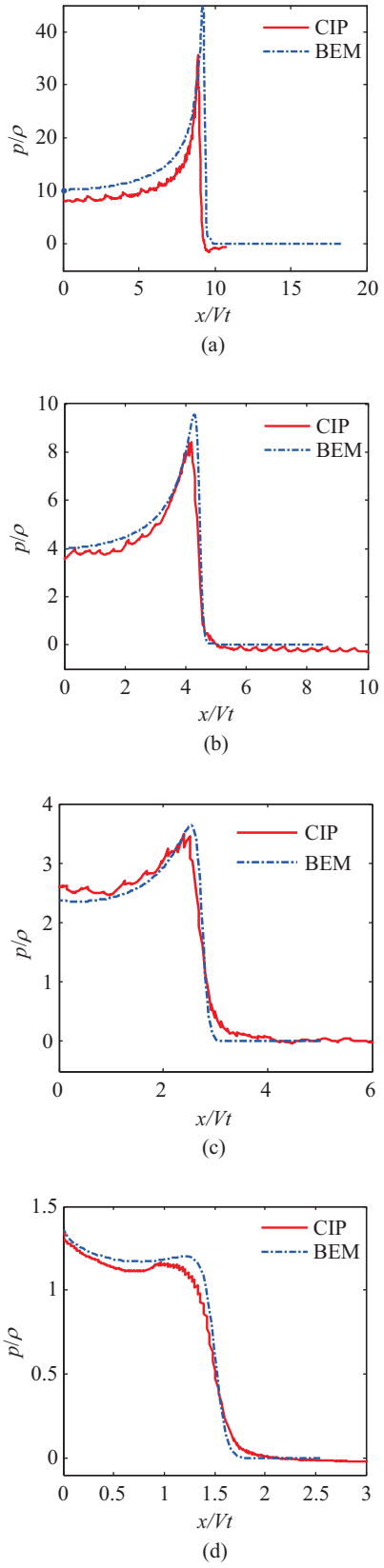

Fig. 4. The comparison of pressure distribution for the wedge entering water with constant speed (CIP: CIP method, BEM: similarity solution by the BEM). (a) $\beta = 10°$, (b) $\beta = 20°$, (c) $\beta = 30°$, (d) $\beta = 45°$.

to $\beta = 10°$, 20°, 30° and 45°. In the BEM, the gravity of fluid was ignored and the impact speed was constant. As there was no flow separation, it led to a self-similar solution. Furthermore, the mass of the structure was also ignored. Fig. 4 gives the pressure distribution over the wedges surface before the flows separated from the side face of the wedges. In Fig. 4, the pressure distribution has been non-dimensionalized by ρV^2, where ρ is the density of water, $V = 1.0$ m/s is the vertical velocity for all wedges. Good agreement with BEM method was evident. In particular, as the linear jet approximation was used in the BEM (Wu et al., 2004) simulation, the pressure in the long and thin jet was zero, resulting in the absence of spike and oscillation. However, the CIP simulation presents a multiphase problem. Each grid cell was filled with air, fluid and solid phase. When solving the Poisson equation, the pressure was calculated over the whole computational domain, thus the pressure value exists in each cell. Therefore the pressure distribution in the jet for the CIP method was not zero. On the other hand, as the SOR (successive over relaxation) iteration method was used to solve the pressure, the divergence caused by the iteration number and the accuracy resulted in the saw teeth behavior of these pressure curves, as shown in Fig. 4.

Fig. 5 gives the wave elevation for four different deadrise angles by CIP method. It was found that as the wedge with small deadrise angle impacts the water surface; the jetting was very thin and moves with very high speed. There were some spikes and oscillations formed along the free surface. This was because the surface tension was not considered in the simulation, thus the free surface easily broke.

2. Test Cases of Water Entry of Wedges in Free Fall with One Degree of Freedom

The cases of free-falling wedges impacting the water surface with one degree of freedom were also investigated and compared with the results from two other experiments.

The first experiment was carried out by Wu et al. (2004). In the experiment, both the acceleration and the strain were recorded. Here, only the former was used to validate the numerical simulation. The V-shaped model is $L = 60$ cm long and $B = 20$ cm wide, as shown in Fig. 6. The model was set up along a steel made gliding platform. When released, the wedge would glide into a tank with the dimensions of 1.65 m × 0.80 m × 1.45 m. In their experiment, friction between the gliding platform and the wedge frame were considered. The acceleration g_e of wedge was not equal to the gravitational acceleration, even before the impact occurred, and hence was taken into account in the analysis.

The second experiment was carried out by Xu et al. (1998). Both the symmetric and asymmetric drop tests were investigated, with the wedges released freely into the water. In this section only the symmetric cases were analyzed. The main interest in such a physical problem came from the need to understand the dynamic response of high-speed ships during water impacts so as to reduce the hull damage resulting from boat slamming (Okada and Sumi, 2000).

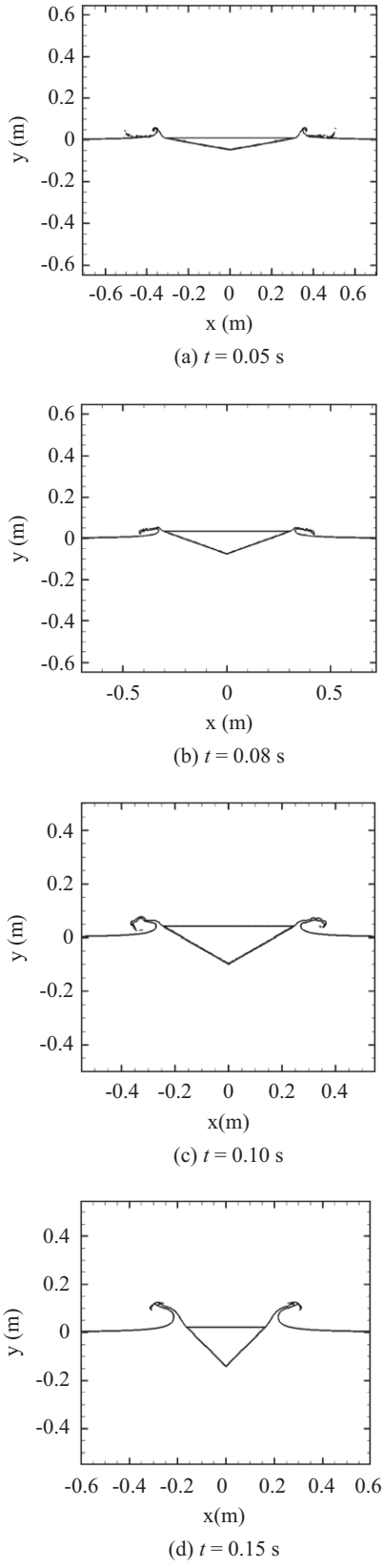

Fig. 5. The free surface deformation for the wedge entering water with constant speed (a) β = 10°, (b) β = 20°, (c) β = 30°, (d) β = 45°. Images represent t = 0.05 s, 0.08 s, 0.10 s and 0.15 s after impact, respectively.

Table 1. Parameters of the configurations studied.

Name	Sym-light	Sym-light	Asym-light
H (m)	0.61	1.22	0.61
α	0°	0°	5°
M_s (kg)	122	122	124
CG (m)	—	—	0.216
I_G(kg m^2)	—	—	8.85

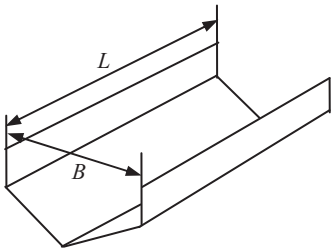

Fig. 6. Model of a V-shaped body.

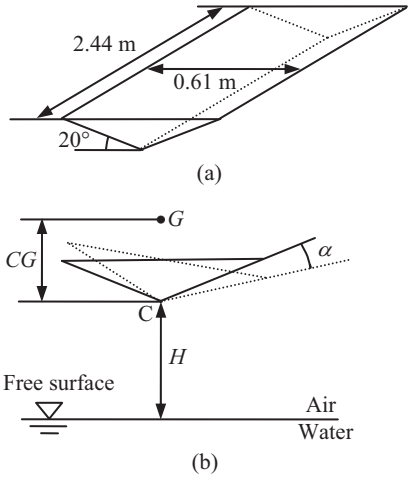

Fig. 7. Experimental configuration of drop tests (a) Geometry of the prismatic hull, (b) Experimental parameters.

The physical model was a high-aspect-ratio prismatic wedge with deadrise angle of β = 20°, as illustrated in Fig. 7(a). Different experimental configurations of drop height H, wedge mass M_S, and heel angle α (Fig. 7(b)) were considered and is summarized in Table 1. For the asymmetric tests, the position of the center of gravity (G) and the inertia were also important parameters, hence the roll and vertical acceleration time-history were recorded by instruments with accelerometers.

Fig. 8 shows the curves of acceleration α (m/s^2) against time $t(s)$, the deadrise angles of the wedges are β = 45° and 20°, respectively. The acceleration of the wedges had been non-dimensionalized by gravitational acceleration, g. For the cases with deadrise angle of β = 20° (Fig. 8(c, d)), the simulation curves and the experiment curves are in excellent agreement, while there are small discrepancies at the later stage for the cases of β = 45° (Fig. 8(a, b)). This could be

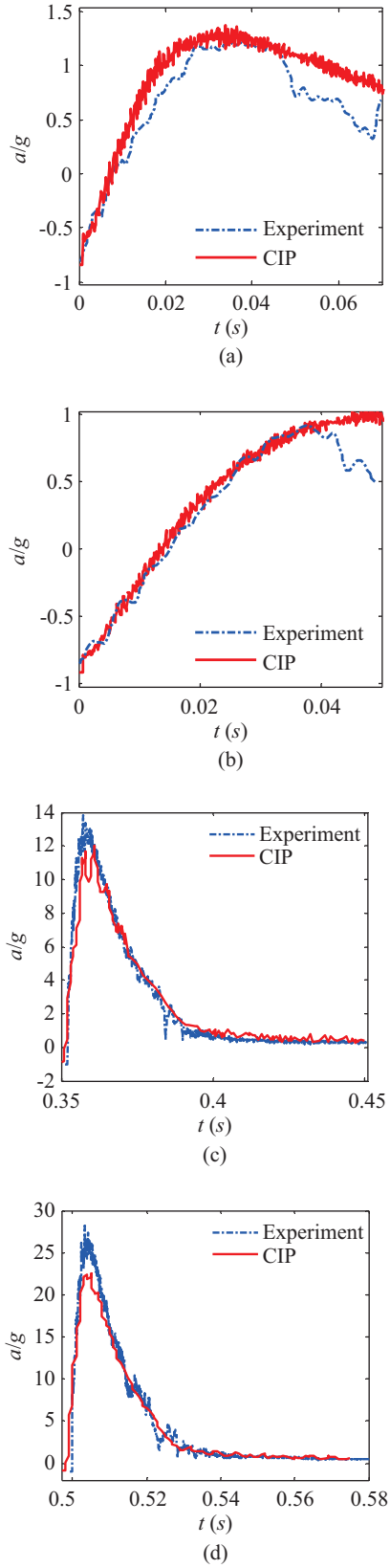

Fig. 8. Acceleration at $\beta = 45°$: (a) $g_e = 8.2015$ m/s^2, $M_b = 13.522$ kg, $V_s = 1.5797$ m/s, (b) $g_e = 8.9716$ m/s^2, $M_b = 30.188$ kg, $V_s = 1.6967$ m/s, and $\beta = 20°$: (c) $g_e = 9.8$ m/s^2, $M_b = 124.0$ kg, $V_s = 3.4577$ m/s, (d) $g_e = 9.8$ m/s^2, $M_b = 124.0$ kg, $V_s = 4.8900$ m/s.

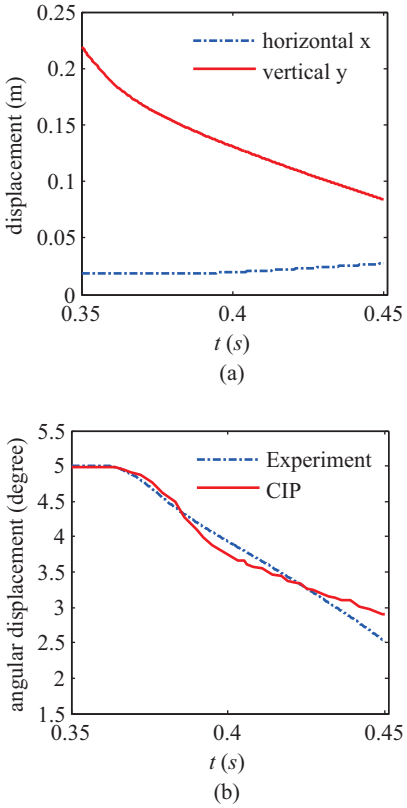

Fig. 9. Displacement of the wedge with the deadrise angle of $\beta = 20°$, heel angle of $\alpha = 5°$, and the released height is $H = 0.61$ m. (a) Horizontal of x and vertical displacement of y, (b) Rotational displacement.

explained by the wedge being pulled to a stop towards the end of the impact (Wu et al., 2004), in which the pulling force was not included in the CIP simulation. Another important factor affecting the comparison is the end effect. In the CIP simulation, it was a completely 2D problem. However in the experiment, as the wedge enters the water, only the middle of the wedge is a 2D problem, but not at the two ends. Similar to the pressure curves, the acceleration curves also showed obvious spike and saw tooth behavior due to divergence of SOR iteration method and accuracy.

3. Test Case of Water Entry of a Wedge in Free Fall Motion with Three Degrees of Freedom

In this section, the wedge in Fig. 7(b) was released freely into the water with complete three degrees of freedom. The whole dynamics of the wedge was governed by both the interactions with water and gravity. The main difficulty that was encountered here is the coupling appearing between linear and angular accelerations, because the flows around the wedge are asymmetric. The deadrise angle of the wedge was $\beta = 20°$, while the heel angle was $\alpha = 5°$, as shown in Fig. 7(b). The wedge was released from a height of $H = 0.61$ m, thus the initial vertical velocity was $V = 3.41$ m/s and the initial horizontal velocity was $U = 0.0$ m/s. To limit the CPU processing time,

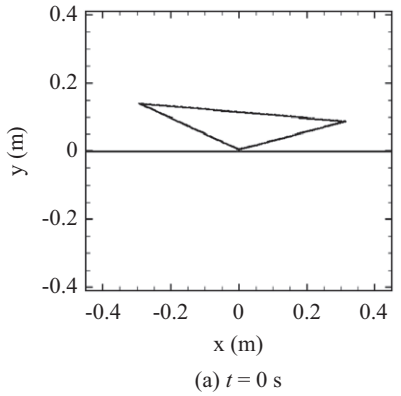

(a) t = 0 s

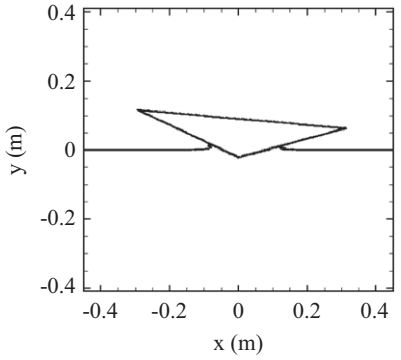

(b) t = 0.0088 s

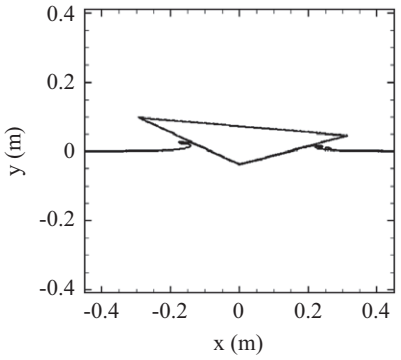

(c) t = 0.0187 s

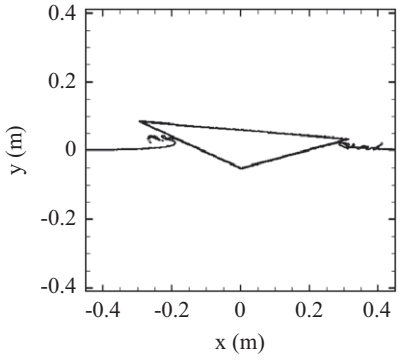

(d) t = 0.0275 s

Fig. 10. Free surface profile of the wedge with the deadrise angle of β = 20°, heel angle of α = 5°, and the released height is H = 0.61 m. At the time of t_0 = 0 s, the wedge touches the water surface.

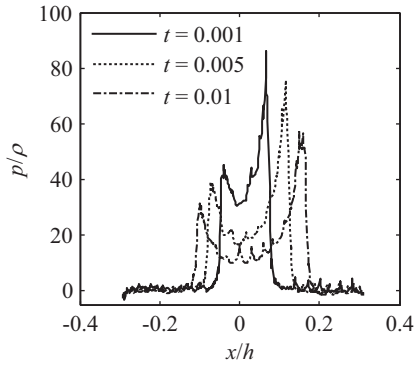

Fig. 11. Pressure distribution evolution of the wedge at the same time corresponding to the case in Fig. 10, at the time of t_0 = 0 s, the wedge touches the water surface.

the free fall motion was not computed. The wedge was placed at a small height just above the free surface at the beginning of the simulation, and the initial kinematic conditions for the CIP wedge were corresponded as much as possible to those in the experiment.

Fig. 9(a) gives the time history curves of horizontal and vertical displacement for the wedge. As the initial heel angle caused the wedge to rotate, the horizontal displacement also increased. The effect of the initial heel angle on the vertical displacement was much smaller. In Fig. 9(b), the rotational angle displacement was compared with that of the experiment. Although there were some discrepancies, the overall trend agreed well. All these show that the interactions between the three degrees of freedom are important during the free fall motion.

Fig. 10 shows the free surface deformations at t = 0.0 s, 0.0088 s, 0.0187 s and 0.0275 s, respectively. It provides information on the successive shapes of the two non-symmetrical jetting generated. The presence of fragmentation at the tip of these jetting were also noticed. Fig. 11 presents the corresponding pressure distribution for the free surface deformations in Fig. 10. The initial heel angle and clockwise rotation increased the peak value of pressure on the right-hand side of the wedge. However, the pressure on the left side was reduced. Over time, the flows moved with high speed and climbed up the side face of wedge, thus the width of the pressure distribution increased while the peak value decreased.

Fig. 12(a) shows the time history of the horizontal acceleration. Fig. 12(b, c) shows the comparison of time history curves of vertical and angular acceleration between the CIP and experimental results. It should be noted that because of the errors made in estimating the initial conditions for computation, the CIP results were adjusted to make the curves match. This was to ensure better comparisons between the two results.

Here, the wedge was relatively flat. As there was an initial heel angle of 5°, the true deadrise angle on the right side was 15°. As a result, some non-negligible air effects seemed to occur at the initial stages of impact. Indeed, the progressive

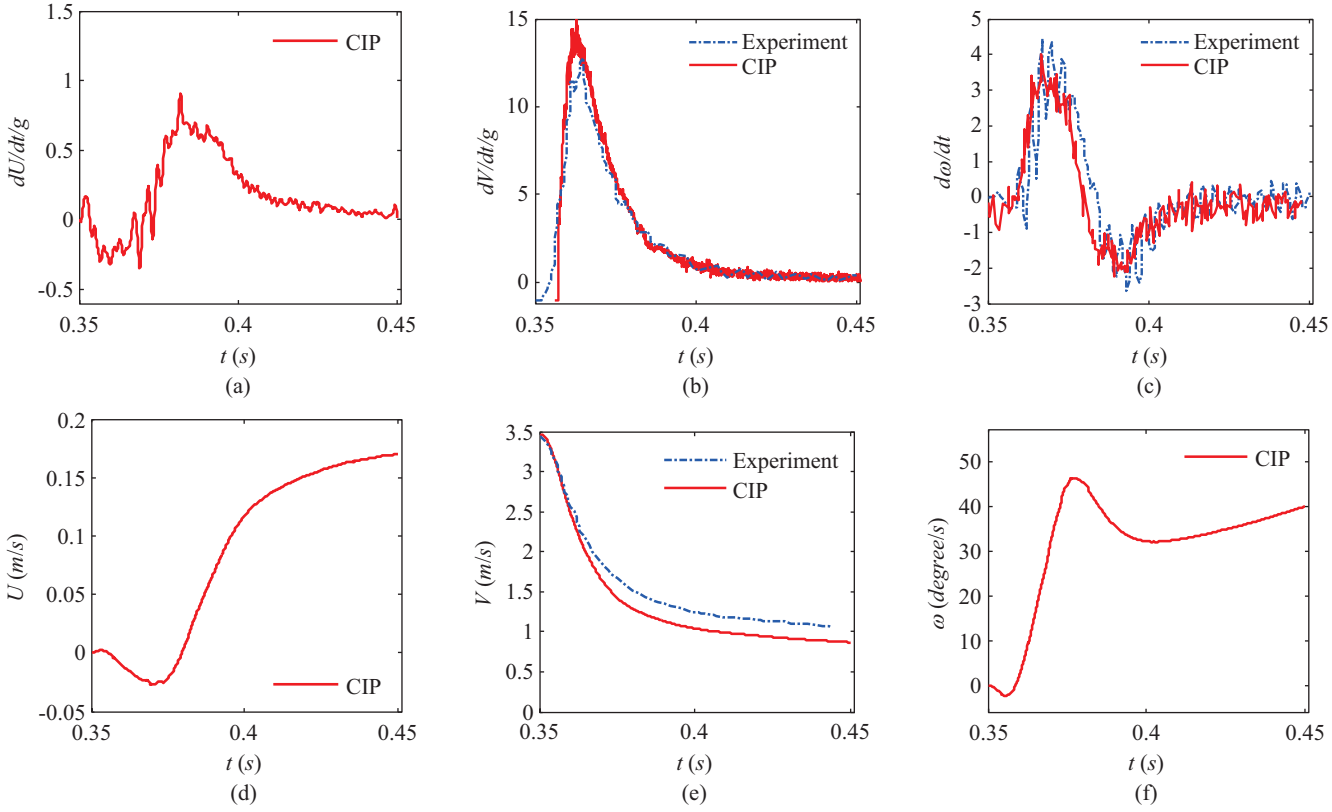

Fig. 12. Motion of the wedge with the deadrise angle of $\beta = 20°$, heel angle of $\alpha = 5°$, and the released height is $H = 0.61$ m.

evolution of the vertical acceleration due to air cushion effects at the initial stage could not be accurately captured by the CIP model. This resulted in a stiffer vertical acceleration slope than that in the experiment. Nonetheless, the amplitude of maximum loads was in good agreement with the experiment. Concerning the time evolution of angular acceleration, some oscillations were noticed on the experimental data. These oscillations were produced by structure vibrations which cannot be captured in the context of rigid body simulations (Xu et al., 1998). These experimental vibrations thus make the comparison with the CIP angular acceleration difficult.

Fig. 12(e) shows the time history of vertical velocity, which showed good agreements between the simulation and experimental results. Fig. 12(f) shows the time history of the angular velocity. As the wedge touches the water surface, the heel angle and the initial impact causes the wedge to rotate clockwise. Then as the pressure on the right half side is much larger than that on the left side, the wedge begins to rotate anticlockwise. This trend also corresponds to the time history curve of horizontal velocity (Fig. 12(d)), where the center of wedge first moves slightly towards the right, and then towards the left, and finally towards the right again.

IV. CONCLUSIONS

The water entry problems of wedges have been solved by a constrained interpolation profile (CIP) based on Cartesian grid method. The simulations include three parts: in section 3.1, the pressure distribution on the wedges as they enter into the water with constant speed are predicted and compared with the similarity solutions by BEM; in section 3.2, the cases of symmetric water entry of wedges in a free fall motion were calculated and the vertical accelerations were also compared with published experimental results; in section 3.3, the water entry of a wedge with an initial heel angle in a free fall motion was calculated, with detailed simulations showing that there are some strong couplings between the three degrees of freedom. For all these three parts, good agreements were found. These results have some importance in applications for practical problems such as ship slamming, which will be further investigated in future works.

ACKNOWLEDGMENTS

The authors would like to thank the support of the Project Funded by the Priority Academic Program Development of Jiangsu Higher Education Institutions (PAPD).

REFERENCES

Dobrovolskaya, Z. N. (1969). Some problems of similarity flow of fluid with a free surface. Journal of Fluid Mechanics 36, 805-829.

Godunov, S. K. (1959). Finite difference methods for numerical computation of discontinuous solutions of the equations of fluid dynamics. Matematicheskii Sbornik 47, 271-295.

Hu, C. H. and M. Kashiwagi (2004). A CIP-based method for numerical simulations of violent free surface flows. Journal of Marine Science and Technology 9, 143-157.

Hu, C. H. and M. Kashiwagi (2009). Two-dimensional numerical simulation and experiment on strongly nonlinear wave-body interactions. Journal of Marine Science and Technology 14, 200-213.

Kihara, H. (2004). Numerical modeling of flow in water entry of a wedge. Proceeding of 19th International Workshop on Water Waves and Floating Bodies, Cortona, Italy, 28-31 March.

Kleefsman, K. M. T., G. Fekken, A. E. P. Veldman, B. Iwanowski and B. Buchner (2005). A volume-of-fluid based simulation method for wave impact problems. Journal of Computational Physics 206, 363-393.

Oger, G., M. Doring, B. Alessandrini and P. Ferrant (2006). Two-dimensional SPH simulations of wedge water entries. Journal of Computational Physics 213, 803-822.

Okada, S. and Y. Sumi (2000). On the water impact and elastic response of a flat plate at small impact angles. Journal of Marine Science and Technology 5, 31-40.

Semenov, Y. A. and A. Iafrati (2006). On the nonlinear water entry problem wedges. Journal of Fluid Mechanics 547, 231-256.

Von Karman, T. (1929). The impact of seaplane floats during landing. NACA TN 321, October, Washington.

Wagner, H. (1932). Uber Stoss-und Gleitvorgange an der Oberfluche von Flussigkeiten. Zeitschrift für Angewandte Mathematik und Mechanik 12, 193-215.

Wu, G. X., H. Sun and Y. S. He (2004). Numerical simulation and experimental study of water entry of a wedge in free fall motion. Journal of Fluids and Structures 19, 277-289.

Xiao, F., Y. Honma and T. Kono (2005). A Simple Algebraic Interface Capturing Scheme Using Hyperbolic Tangent Function. International Journal for Numerical Methods in Fluids 48, 1023-1040.

Xu, G. D., W. Y. Duan and G. X. Wu (2008). Numerical simulation of oblique of an asymmetrical wedge. Ocean Engineering 35, 1597-1603.

Xu, G. D., W. Y. Duan and G. X. Wu (2010). Simulation of water entry of a wedge through free fall in three degrees of freedom. Proceedings of the Royal Society A 466, 2219-2239.

Xu, L. X., A. W. Troesch and R. Petterson (1998). Asymmetric hydrodynamic impact and dynamic response of vessel. Proceedings of 17th International Conference on Offshore Mechanics and Arctic Engineering 98-320.

Yang, J. M. and F. Stern (2009). Sharp interface immersed- boundary/level-set method for wave-body interactions. Journal of Computational Physics 228, 6590-6616.

Yang, Q. Y. and W. Qiu (2012). Numerical simulation of water impact for 2D and 3D bodies. Ocean Engineering 43, 82-89.

Zhao, R. and O. Faltinsen (1993). Water-entry of two-dimensional bodies. Journal of Fluid Mechanics 246, 593-612.

Zhao, X. Z. and C. H. Hu (2012). Numerical and experimental study on a 2-D floating body under extreme wave Conditions. Applied Ocean Research 35, 1-13.

Zhu, X. Y., O. M. Faltinsen and C. H. Hu (2007). Water entry and exit of a horizontal circular cylinder. Journal of Offshore Mechanics and Arctic Engineering 129, 253-264.